Nanostructured carbon materials for hydrogen energetics

Peteris Lesnicenoks[1, 2*], Liga Grinberga[1], Laimonis Jekabsons[1], Andris Antuzevičš[1], Astrida Berzina[2], Maris Knite[2], Gatis Taurins[3], Šarūnas Varnagiris[4], Janis Kleperis[1]

[1]*Institute of Solid State Physics, University of Latvia, Kengaraga Street 8, Riga, LV 1063, Latvia*
[2]*Institute of Technical Physics, Faculty of Materials Science and Applied Chemistry, Riga Technical University, Paula Valdena street 3/7, Riga, LV 1048, Latvia*
[3]*"Keramserviss" LTD, Tauriņi, Adazi, LV 2164, Latvia*
[4]*Centre for Hydrogen energy technologies, Lithuanian energy institute, Breslaujos g. 3, Kaunas, LT-44403, Lithuania*

[*]Corresponding author, Tel: (+371) 29100445; Fax: (+371) 67132778; E-mail: peteris.lesnicenoks@rtu.lv

Received: 27 July 2016, Revised: 28 August 2016 and Accepted: 13 October 2016

DOI: 10.5185/amlett.2017.7088
www.vbripress.com/aml

Abstract

Hydrogen storage is one of the main problems, to catalyse wide hydrogen use in transportation, technology and energetics. Composites involving nanostructured carbon species could be the solution for hydrogen storage problem because of their promising surface/volume relation. Not only catalysis and gas sensing on graphene basis should be considered, but also metal decorated graphene structures for use in hydrogen storage should be an active field for research and development. Heat conductivity and large surface area of graphene-like materials can endorse research for hydrogen storage in low pressures and close to room temperature (RT) conditions - increasing possibility for RT-range devices in hydrogen energetics. For increased hydrogen storage investigations, we propose metal intercalated graphene structures, acquired during synthesis of graphene sheets. Intercalation, or decoration of graphene surfaces and edges have shown possibility to stabilize defects in graphene sheets. Graphene defects have shown to be sensitive against hydrogen gas and might as well prove themselves stable enough to achieve low pressure hydrogen storage. A simple method is proposed for synthesis of graphene sheet stacks (GSS). There is lack of research for synthesis of carbon nanomaterials from industrial graphite waste. Our research for stabilization of electrolyte solution and increased production amounts for hydrogen accepting samples continues.

Keywords: Hydrogen, storage, grapheme, intercalation, recycling.

Introduction

If hydrogen is the most abundant element of the universe, then the carbon is sixth behind it. As hydrocarbons both plays a critical role in the living organisms and ecosystems on Earth, and for thousands of years, has been a source of energy. The humanity evolves burning hydrocarbons with a high carbon content, which has led to irreversibly polluted environment. Now we are wiser and continue to gain energy from fuels that contain less carbon or is completely free from it (hydrogen) [**1**].

Will the Hydrogen economy exclude the carbon from the market altogether? In the case of fuel burning, probably yes (fuel cells and batteries are clean technologies for future energy purposes), but as element in materials to create devices for hydrogen technologies - never. To name for example hydrogen production technologies: water electrolysers, fuel reformers - they cannot be made without carbon in different allotropic forms and dimensions (from 0D to 3D); hydrogen storage technologies: compressed up to 700 bars hydrogen in carbon fibre tanks is in recently commercialized electric/hydrogen cars, research is open for hydrogen solid state storage in different nanostructured carbons; hydrogen energy technologies: proton exchange membrane fuel cell (PEMFC) is mostly based on carbon-containing materials: bipolar plates, electrodes, proton conducting polymer membrane (hydrocarbon polymers cross-linked with fluorine, sulphur or other elements [**2**, **3**].

What is behind nanostructured carbon materials (NCM)? Number of the research articles about "nanostructured carbon materials" in last few decades has grown exponentially. NCM can be classified as various allotropes in 0D (amorphous carbon black and graphitized carbon black), 1D (polymer chains), 2D (graphene) and 3D (diamond) nanoscale. There are up to 100 review articles about their research in different applications. By assembling carbon nanomaterials with functional metal or oxide nanocrystals, composites which have new functions in electrical, physical, or chemical properties are obtained.

Hydrogen storage is one of the main problems, to push forward hydrogen use in technology an energetics. Nanostructured carbon materials could help to find

solution for hydrogen storage problem because of their promising high surface area and pronounced micro-pore volume. Usually graphite waste is either deposited in landfills or made a filler in composite materials. Enforced concrete or plastic matrices are mixed with graphite to increase their mechanical and thermal properties. In some cases, creating electromagnetically shielding construction materials have been found. But even more common is graphite use in slag formation in metallurgy – adding graphite as a sponge like absorber for slag. Also some thermal composite materials can be created. Here we step in with our method. Many of the graphite waste materials can be recycled in exfoliated graphene sheet stacks GSS. Of course, for now, highly irradiated graphite still needs to go to designated landfills. But other forms of graphite, which maintains its sheet structure, can be formed in electrodes for this method and exfoliation can be performed. Mass production of high-quality graphene sheets is essential for their practical application in electronics, optoelectronics, composite materials, and energy-storage devices [**4**]. In our previous work [**5**] industrial waste graphite [**6**] and clean graphite from magnetron sputtering graphite target were used as a source materials and similar exfoliation results were obtained. Regarding hydrogen binding with exfoliated GSS it was shown that decoration with lithium and magnesium increases amount of adsorbed hydrogen at cryogenic temperatures [**5**]. This work is a continuation of our previous researches on hydrogen interaction with graphene exfoliated from waste graphite [**5**] and is devoted to research of influence of vanadium (V) and bismuth (Bi) impurities on properties of (GSS) and hydrogen adsorption capability.

Experimental

Materials/ chemicals details

In our work we use graphite crucibles, from bronze metallurgy, after the end of their working lifetime – waste [6], as a starting material for Graphene Sheet Stack (GSS) synthesis. $VOSO_4$ – vanadyl sulphate, $Bi_2(SO_4)_3$ – bismuth sulphate, DMF – Dimethilformamide, H_2SO_4 – Sulfuric acid 98%, HNO_3 – Nitric acid 20%, Acetone (all from *Sigma Aldrich*)

Material synthesis / reactions

Developed synthesis method consists of waste graphite crucible piece of appropriate size for electrolyte container and Platinum counter electrode to fit in a single synthesis tray. Electrolyte consists of 1 M H_2SO_4 solution (300 ml) and 50 ml of 1 M metal sulphate solution – depending on the desired modification. For example, V_2O_5, $Bi_2(SO_4)_3$ can be added to modify GSS in solution synthesis method. Graphite and platinum electrodes are connected to power source of 10 V and timed switch which changes the direction of passing current. For our purposes 3:5 s pulses of -10 and 10 V for 5 h allows us to exfoliate about 4 g intercalated graphene sheet stacks. Decrease in voltage have been suggested as size determining variable. Unconstrained current helps to get maximum of 5 A at the pike current for our graphite electrode size. Working amperage is about 1.5 A which varies upon evaporating electrolyte or depth of submersion of graphite electrode. Previously little mentioned is the possibility to use two graphite electrodes at pulse frequency 5:5 s. Choice towards similar electrodes leads to increase in working current ~3 A and increase of exfoliated GSS. Product has to be removed periodically from exfoliation chamber to ensure small currents and keeping contacts for electrodes clean and participation in electrolysis. For Bi GSS sample HNO_3/acetone electrolyte was used – to counteract solubility properties – (150 ml/150 ml) in addition to 50 ml of salt solution.

After exfoliation material is vacuum dried and washed from electrolyte at the same time. Dried material then is mixed with DMF/H_2O solution 10:1 in a sealable glass jar, which is further placed in sonication bath for 3+ hours. When sample has been sonicated, and material particles are well stabilized in the solution, sample is vacuum dried again. After second drying sample is placed in a tube furnace – within alumina tube which is purged with Ar/H_2 95:5 gas mix for reduction. Furnace heats sample up to 800 °C. During this heating and washing with inert/reducing gas, our material is cleaned from previous chemical treatments which can detach from sample. We modify edge chemistry, getting rid of CO, COOH, OH, SO_2 groups to allow cleaner surfaces and to allow stronger interactions with hydrogen gas in later experiments.

Characterizations

Material was characterized with:

SEM (*Phenom Pro*) up to 95000x magnification at 10 kV.

EDAX (*Eagle 3*) XRF spectrometer was used in our work. Sample excitation by X-rays (Rh tube) focused by poly capillary fibre lens, minimum spot size 50 microns (fwhm). Energy dispersive liquid N_2-cooled Si detector with Be window, suitable for detecting of XRF of chemical elements ranging from Na to U.

Raman (*Renishaw InVia*) green laser (514 nm, max power 20 mW), objective x100, laser power used 100%, 30 – 4000 cm^{-1} exposure time 10 s; red laser (633 nm, max power 12.5 mW) objective x100, laser power used 100%, 30 –4000 cm^{-1} exposure time 10 s.

The main **XPS** (*PHI 5000 Versaprobe*) parameters were: monochromated 1486.6 eV Al radiation, 25 W beam power, 100 μm beam size, and 45° measurement angle. Survey scan was performed using 115 eV energy throughput, 1 eV step; spectra of individual elements were recorded with 23.5 eV energy throughput, 0.1–0.2 eV step for 20–35 eV window (depending on element). Sample charging was compensated using a dual neutralization system consisting of low energy electron beam and ion beam. Energy calibration was done by measuring C1s peak of anthropogenic carbon and fixing it at 284.8 eV. XPS spectra processing and analysis was done using Multipak software and NIST Standard Reference Database.

Conductivity measurements - The temperature control system Linkam THMSE 600 coupled with an Agilent 34970A data acquisition unit was used for electrical resistance measurements of the graphene sheet stacks powder samples during the heating and the cooling. The powder sample was compressed in special home-made mini-chamber by screwing in brass cylinder as shown in **Fig. 2s**. To reduce the temperature gradient in the sample, the Linkam THMSE 600 heating/freezing stage chamber was modified with a 3 mm thick brass cap that was used to cover the samples during measurements. The temperature under the cap and near to the sample was measured with a Pt–Rh thermocouple. Since the samples had very low electrical resistivity the resistance measurements were performed using a Kelvin (4- wire) resistance measurement method.

PVT/MS (Sieverts type device + RGA 100) uses stainless steel sample chamber and vacuum system which is coupled with quadrupole mass spectrometer (MS) RGA 100 – sensitive up to ionic-atomic mass 100. Samples are heated and vacuumed up to 473 K then system is filled with He gas to determine material volume. Usual Sievert's process is applied performing measurements at H_2 atmosphere and temperature interval LN to 573 K (300 °C).

EPR measurements were made using a conventional X-band (≈9.10 GHz with 0.01 GHz accuracy) spectrometer RE 13-06 with 100 kHz field modulation at 77 K by submerging samples in a cold-finger Dewar filled with liquid nitrogen. The magnetic field calibration was done using a polycrystalline DPPH standard with $g = 2.0036 \pm 0.0001$.

Results and discussion

Shortly after synthesis SEM and XRF (EDAX) experiments were performed to determine topography and morphology of our material. We found that our material has exfoliated in sheet stacks with sheet thickness from 20 nm to several microns. Elsewhere in literature similar structures have been produced by different methods [**7**, **8**] and have been named xGNP - exfoliated Graphite nanoplatelets or GS - Graphite Stacks, but in our SEM experiments we saw nano- level structures as well as macro-pores thus we are not completely sure, if it is the same material as in mentioned literature, yet it exhibits similar properties based on the Raman spectra. Our synthesis method is cyclical – providing exfoliation – reduction cycles. This means shorter reduction time is needed than for purely chemically exfoliated graphene, applying the same reduction method.

As it can be seen from SEM images **(Fig. 1. a-d),** an exfoliation of raw monolithic graphite is done and layer stacks produced. Stack dimensions exceed 100 μm and partly open-layer structures presents **(Fig. 1. a).** In largest magnification images we can see **(Fig. 1. b)** that the layer thickness of stacks is 123 nm what corresponds to 120 graphene sheets (thickness of one sheet is between 0.4 and 1.7 nm [**9**, **10**]. Decoration of stack layers with nanocrystals from the traces of impurities in source material and/or salts in selected electrolytes in exfoliation process are shown in **Fig. 1. c** and **d**.

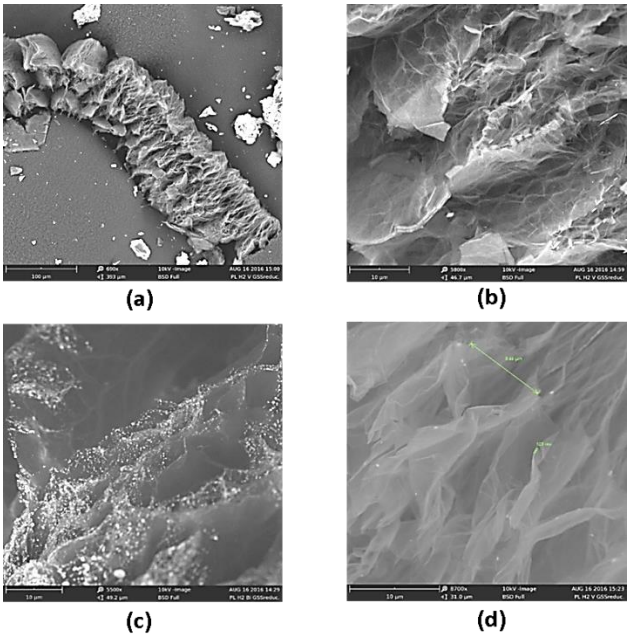

Fig. 1. SEM images of (a) V GSS after reduction - macroparticle, (b) V GSS after reduction, (c) Bi intercalated GSS sample after reduction, (d) V GSS after reduction – pore and sheet size.

XPS measurements showed that, graphene consists of carbon of 91.6 atomic %, oxygen - 6.8 atomic % and silicon - 1.6 atomic % **(see Fig. 2. survey graph)**. XPS fitted C1s peak consist of sp^2 bond at binding energy 285.0 eV, sp^3 at binding energy 285.7 eV (both peaks correspond to C=C compound) and C-OH bond at 286.6 eV [10]. The Si2p was fitted with two peaks at 100.4 and 102.8 eV. They are related to silicon sub-oxide Si^{+1} (SiO), in which silicon atoms are connected to one oxygen atom and silicon dioxide Si^{+4} (SiO_2), respectively. The same result was observed with O1s, where O^{+2} (SiO_2) and O^{+1} (SiO) peaks were observed. In both cases area ratio approximately was the same (9:1). Also the presence of C-OH compound in O1s peak was confirmed in C1s fitting results [11]. Additional information of fitted peak is shown in **Table 1** [**12**].

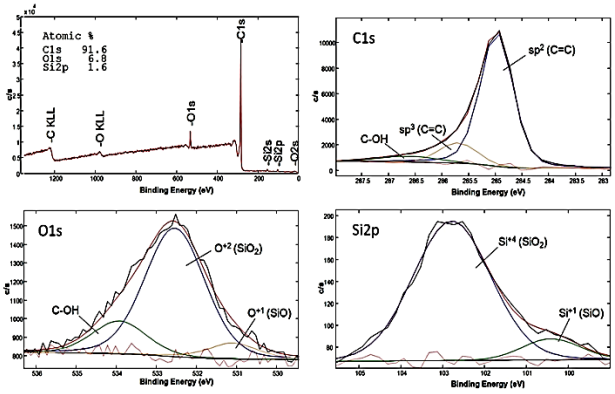

Fig. 2. XPS results: survey with atomic concentration and fitted peaks: C1s, O1s and Si2p peaks. Black lines – measured peaks, red lines – calculated peaks. Dashed lines show difference between measured and calculated lines.

Table 1. Information of XPS fitted C1s, O1s and Si2p peaks.

Peak	Chemical state	Binding energy, eV	FWHM, eV	Area, %
C1s	sp^2 (C=C)	285.0	0.72	81.4
	sp^3 (C=C)	285.7	0.85	13.0
	C-OH	286.6	1.28	5.6
O1s	O^{+1} (SiO)	531.1	1.45	8.6
	O^{+2} (SiO_2)	532.5	1.77	74.2
	C-OH	533.9	1.58	17.2
Si2p	Si^{+1} (SiO)	100.4	2.10	10.0
	Si^{+4} (SiO_2)	102.8	1.66	90.0

EDAX experiments show that our samples consist of following impurities – Si, S, Zn, V, Fe, but light elements are not visible in this experiment.

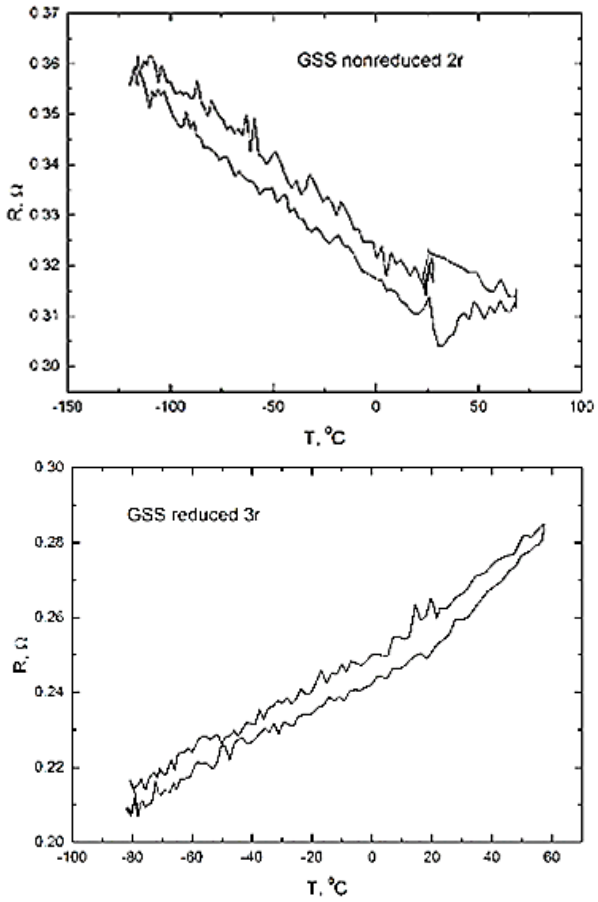

Fig. 3. Resistance measurements of (a) GSS sample before reduction, (b) GSS sample after reduction in Ar/H_2 flow in tubular furnace.

Combining XPS with EDAX data, we can determine composition of samples to be approximately 1.6% Si, 0.185% S, 0.183% Fe, 0.014% V, 0.111% Bi, 0.003% Zn, and about 6.4 at% O. Percentage varies between V and Bi samples. The electrical resistance of GSS samples before reduction **(Fig. 3. a)** decreases and of GSS samples after reduction **(Fig. 3. b)** increases with temperature, indicating negative and positive temperature coefficients of resistance accordingly. There are number of publications about resistance or conductivity dependence on temperature in different NCM: single-layer graphene (SLG), few-layer graphene (FLG), graphene nanosheets (GNs) and others (see, for example [**13**]) but reported results from different authors differ and sometimes are contradictory. From theoretical considerations [**13**] follows, that the conductivity of graphene increase with the increase in temperature, in which the increase rate decreases as temperature increases. Decrease of conductivity from temperature is observed for graphene oxide [**14**]. In our case based on C. Punckt *et al.* work [**15**] we consider semiconductor like conductivity for GSS sample before reduction due to presence of graphene oxide, but reduced GSS showed metal like conductivity. As developed in [**15**] "the transition from a semiconducting to metallic behaviour when proceeding from graphene oxide to reduced graphene is related to increase of size and number of sp^2 – hybridised domains with further reduction, until eventually a percolated sp^2 path network forms within a background of sp^3 – hybridized area". Before the percolation transition occurs, the hopping conductivity between adjacent sp^2 domains separated by non-reduced sp^3 nano-regions take place [**15**] and the resistance decreases versus temperature as shown in **Fig. 3.a**. After reduction the diffusive motion of electrons in sp^2 area is limited by scattering at functional groups and lattice defects [**15**] and R slightly rises versus T as one can see in **Fig. 3.b**.

Raman spectra of our samples reveal good reduction influence – visible in red laser. Comparison between red and green laser Raman spectra can be done using supplementary data (**Fig. 1s**). In short, green laser (514 nm) shows D peak shift right, and 2D peak shift left, along Raman shift axis. G peak remains almost unchanged (Table 1s). Graphene peak intensity ratio

I_G/I_{2D} remains in region of 1 for reduced V GSS, while being larger for non-reduced V GSS and all of the Bi GSS samples, reaching 1.88 for Bi GSS with green laser and 2.57 with red laser excitation. All of the calculated I_G/I_{2D} with red laser excitation are larger than those obtained with green laser.

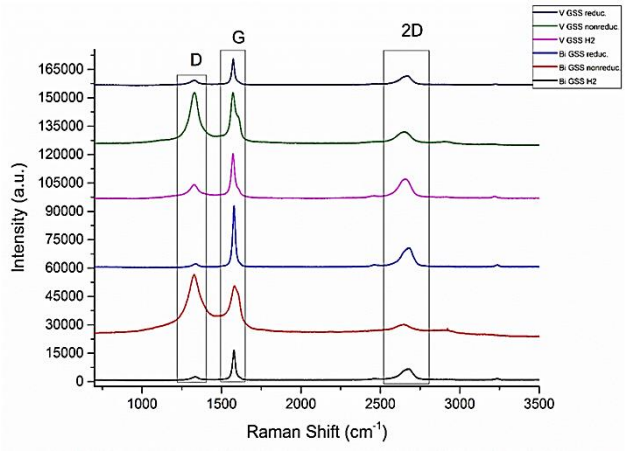

Fig. 4. Raman spectra (633 nm) of (top to bottom): 1) V GSS after reduction in 800°C for 3 hours, 2) V GSS sample before reduction, showing highly agglomerated defective structure, 3) V GSS after H_2 sorption experiments, 4) Bi GSS after reduction procedure, 5) Bi GSS non-reduced sample, 6) Bi GSS after H_2 measurements.

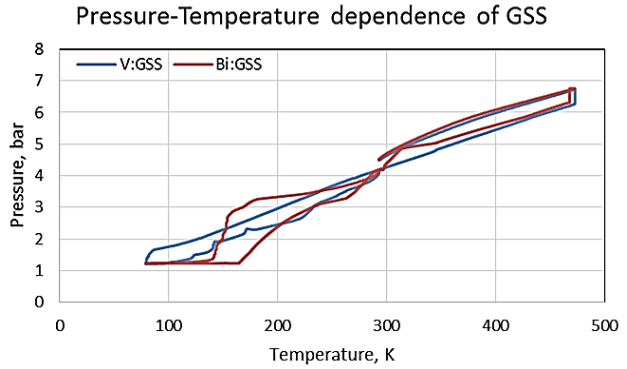

Fig. 5. Bi GSS hydrogen desorption characteristics and V GSS desorption characteristics.

As it is seen from **Fig. 5.** adsorption/desorption curves of V GSS and Bi GSS are similar (exception is that Bi has impurity enhanced adsorption/desorption at selected temperatures – adsorption starts at 300 K (first phase) and desorption at 140 K. Amount of maximal adsorbed hydrogen does not exceed 0.15 wt%, likely as for GSS without impurities [**5**].

As it is seen from **Fig. 6.** all measured samples are characterized by more or less pronounced wide envelope curve without more detailed structure that runs through the entire EPR spectrum. It's likely to come from the paramagnetic agglomerates with different concentrations in various samples, because of the source material. Similar broad signals are observed for graphene oxide (GO) samples reduced in paraffin and associated with the ferromagnetically coupled spins on zig-zag edges in small magnetic clusters [**16**]. In all spectra **(Fig. 6.)** narrow structure at 3250 G with $g \approx 2$ consists of two lines – the first closer to g = 2 is typical for carbon materials (graphite, graphene, nanotubes etc.) and may be ascribed to C-related dangling bonds of spin S = ½ each [**17**]. Second line (closer to g = 1.98) is sensitive to processing procedures (reduction in Ar/H_2 atmosphere, hydrogen sorption/desorption), but the origin of it requires further studies. As synthesized GSS with vanadium **(Fig. 6. (c))** has pronounced structure of fine lines around central line, coming from vanadium V^{+4} ion – electron with spin 1/2 interacting with nuclear spin from ^{51}V 7/2 could create at least 8 lines with a similar structure [**18**]. Treatment of V GSS sample in reductive atmosphere leads to the disappearance of the fine structure lines, suggesting that vanadyl ion is transformed to a lower valence state.

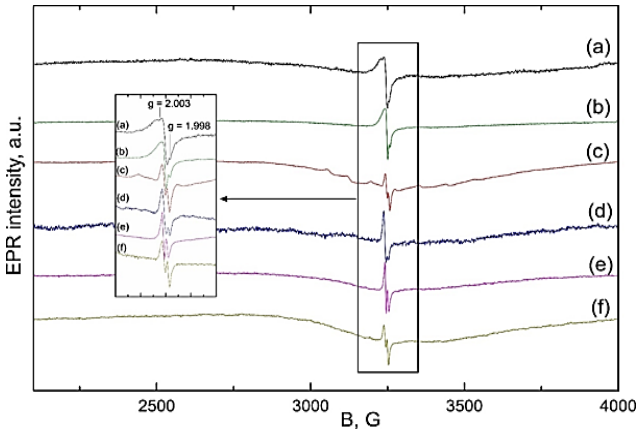

Fig. 6. EPR a) Non-reduced GSS b) Bi GSS non-reduced. c) V GSS non-reduced d) V, Bi GSS reduc., e) V GSS reduc., f) V GSS H_2.

Conclusion

We have developed and improved Graphene Sheet Stack (GSS) synthesis method by recycling metallurgy waste. During GSS synthesis we have successfully modified the samples with V and Bi as is shown by EDAX measurements. After H_2 sorption experiments we can conclude that our samples are not behaving desirably at RT range up to 6 bar pressure for hydrogen solid state storage, but Bi as impurity enhanced adsorption/ desorption at 300 K/140 K up to 0.15 wt%. EPR spectra analysis and Raman spectra shows that our samples are highly defective at some points, and that reduction in Ar/H_2 atmosphere is needed in spite of our electrochemical synthesis method, which include reduction cycle too. This is supported by electrical conductivity measurements showing well visible property change from semiconducting to metallic conduction behaviour. Intercalation GSS with Bi during synthesis process could prove itself to be most useful – it causes higher percentage of ion intercalation and higher I_G/I_{2D} peak intensity ratios in Raman spectra (more expressed interlayer separation).

Acknowledgements

Authors greatly acknowledge National Research Program IMIS[2] and and LCP Project no. 666 for financial support. Keramserviss LTD for raw material – to investigate recyclability of graphite waste. To all coauthors and Institutions for encouragement to succseed in scientific research.

Author's contributions

Conceived the plan: LG, PL, JK, GT; Performed the experiments: AA, AB, PL, ŠV, LJ; Data analysis: AA AB, JK, PL, ŠV; Wrote the paper: PL, JK, MK, AB. Authors have no competing financial interests.

References

1. Goede, A.; van de Sanden, R.; *Europhys. News*, **2016**, *47*, 22. **DOI:** 10.1051/epn/2016304.
2. Hoffmann, P.; Tomorrow's energy : hydrogen, fuel cells, and the prospects for a cleaner planet; The MIT Press: USA, **2012**.
3. EUROPEAN COMMISSION, A Roadmap for moving to a competitive low carbon economy in 2050; **2011**. **URL:** http://eur lex.europa.eu/legal-content/EN/ALL/?uri=celex%3A52011DC0112.
4. Parvez, K.; Wu, Z.-S.; Li, R.; Liu, X.; Graf, R.; Feng, X.; Müllen, K.; *J. Am. Chem. Soc.*, **2014**, *136*, 6083. **DOI:** 10.1021/ja5017156.
5. Lesničenoks, P.; Zemītis, J.; Kleperis, J.; Čikvaidze, G.; Ignatāns, R.; *Rigas Teh. Univ. Zinat. Raksti, Ser. 1*, **2015**, *31*, 21. **DOI:** 10.7250/msac.2015.004
6. Keramserviss LTD; Graphite Crucibles; **2016**. **URL:** http://www.keramserviss.lv/public/index.php?lang=lv&section=312.
7. Atul Tiwari, Ashutosh Tiwari (Eds), Bioengineered Nanomaterials, CRC Press, USA, **2013**.
8. Hardwick, L.J.; Buqa, H.; Holzapfel, M.; Scheifele, W.; Krumeich, F.; Novák, P.; *Electrochim. Acta*, **2007**, *52*, 4884. **DOI:** 10.1016/j.electacta.2006.12.081.
9. Shearer, C.J.; Slattery, A.D.; Stapleton, A.J.; Shapter, J.G.; Gibson, C.T.; *Nanotechnology*, **2016**, *27*, 125704. **DOI:** 10.1088/0957-4484/27/12/125704.
10. Siokou, A.; Ravani, F.; Karakalos, S.; Frank, O.; Kalbac, M.; Galiotis, C.; *Appl. Surf. Sci.*, **2011**, *257*, 9785. **DOI:** 10.1016/j.apsusc.2011.06.017.
11. Jelenković, E.; To, S.; Blackford, M.; Kutsay, O.; Jha, S.; *Mater. Sci. Semicond. Process.*, **2015**, *40*, 817. **DOI:** 10.1016/j.mssp.2015.07.085.
12. Moulder, J.F.; Chastain, J.; King, R.C.; Handbook of x-ray photoelectron spectroscopy : a reference book of standard spectra for identification and interpretation of XPS data, Physical Electronics: USA, **1995**.
13. Fang, X.-Y.; Yu, X.-X.; Zheng, H.-M.; Jin, H.-B.; Wang, L.; Cao, M.-S.; *Phys. Lett. A*, **2015**, *379*, 2245. **DOI:** 10.1016/j.physleta.2015.06.063.
14. Muchharla, B.; Narayanan, T.N.; Balakrishnan, K.; Ajayan, P.M.; Talapatra, S.; *2D Mater.*, **2014**, *1*, 11008. **DOI:** 10.1088/2053-1583/1/1/011008.
15. Punckt, C.; Muckel, F.; Wolff, S.; Aksay, I.A.; Chavarin, C.A.; Bacher, G.; Mertin, W.; *Appl. Phys. Lett.*, **2013**, *102*, 023114. **DOI:** 10.1063/1.4775582.
16. Majchrzycki, L.; Augustyniak-Jablokow, M.A.; Strzelczyk, R.; Ma¢kowiak, M.; *Acta Phys. Pol., A*, **2015**, *127*, 540. **DOI:** 10.12693/APhysPolA.127.540.
17. Rao, S.S.; Stesmans, A.; Wang, Y.; Chen, Y.; *Phys. E (Amsterdam, Neth.)*, **2012**, *44*, 1036. **DOI:** 10.1016/j.physe.2011.07.019.
18. Amarande, L.; Miclea, C.; Cioangher, M.; Grecu, M.N.; Pasuk, I.; *J. Alloys Compd.*, **2016**, *685*, 159. **DOI:** 10.1016/j.jallcom.2016.05.266.

Supplementary information

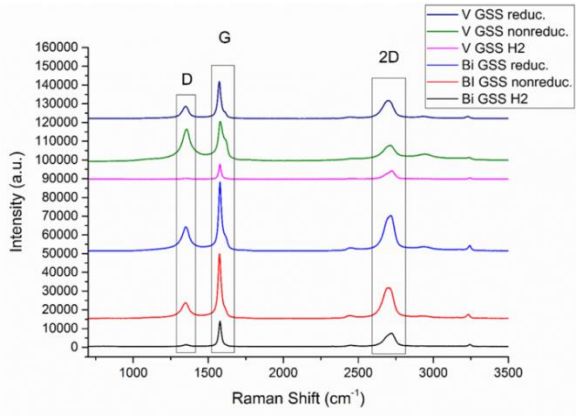

Fig. 1s. Raman spectra of GSS samples in 514 nm laser.

Table 1s. Raman peak intensities.

Sample	Green 514nm			Red 633nm		
	D	G	2D	D	G	2D
V GSS reduc.	1348	1575	2699	1326	1573	2671
V GSS non reduc.	1356	1582	2714	1326	1572	2646
V GSS H_2	1348	1580	2722	1333	1581	2685
Bi GSS reduc.	1348	1580	2707	1340	1578	2682
Bi GSS non-reduc.	1348	1575	2699	1326	1578	2672
Bi GSS H_2	1353	1581	2721	1333	1578	2675

Table 2s. Raman peak intensities for I_G/I_{2D}.

Sample	I_G/I_{2D}	
	Green	Red
V GSS reduc.	1.07	1.08
V GSS non-reduc.	1.11	1.24
V GSS H2	1.02	1.06
Bi GSS reduc.	1.24	1.49
Bi GSS non-reduc.	1.55	1.67
Bi GSS H2	1.88	2.57

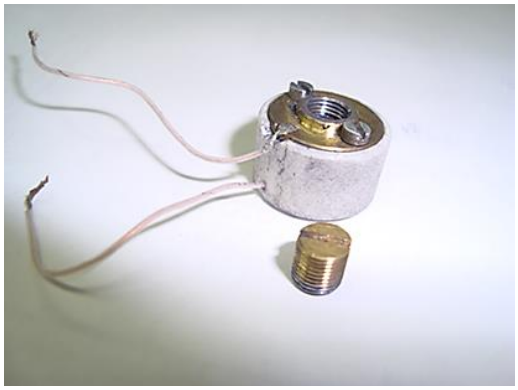

Fig. 2s. Home-made mini-chamber for nanopowder electrical resistivity measurements.

As it is shown in Table, usually pristine monolayer graphene like structures are characterised. Recycled graphite for hydrogen storage has not been considered before. Similar materials can be found – our results are consistent with data obtained by others, where applicable.

H.K. Seo suggests following - $I_D/I_G < 0.2$ low value suggests that the graphene layer has few surface defects. The number of layers and the uniformity of graphene over this area were also illustrated by Raman mapping of the 2D-to-G peak intensity ratio (I_{2D}/I_G) (**Fig. 3c**). Raman mapping of I_{2D}/I_G indicated that the multi-layer graphene consisted of mono-layer to few-layer portions (**Fig. 3d**), and that ~90% of the surface had I_{2D}/I_G ~0.7, which is the signature of three-layer graphene. In the average Raman spectrum, the 2D peak had full width at half-maximum of ~58 cm−1 and I_{2D}/I_G of ~0.62; these values are similar to those of three-layer graphene grown using CVD [**S1**].

Table 3s. Properties of graphene sheet stacks – comparison with results from supplementary literature [**16, S1-S4**].

Data source and preparation method	Morphology SEM	Composition XPS, at %	Composition XPS+EDAX	Resistance, Ω, 4-wire probe	Hydrogen adsorption /desorption	Raman spectra, laser 514 nm	EPR spectra
This research, electrochemical cyclic exfoliation	Thickness of sheets up to 20 nm; stack dimensions 100 μ and thickness up to 123 nm	C – 91.6 O – 6.8 Si – 1.6 C=C, C-OH, Si-O and Si-O- bonds;	1.6% Si, 0.185% S, 0.183% Fe, 0.014% V, 0.111% Bi (or V), 0.003% Zn, and about 6.4 at% O	0.2 – 0.3; change from semiconducting (as obtained) to metallic (after reduction) conduction behaviour	Adsorption start at 300 K, desorption above 140 K; maximal amount 0.15 wt%	Peaks, cm-1 D – 1348-1356; G – 1575-1582 2D – 2699-2722	$g \approx 2$; $g = 1.98$
[16] Majchrzycki, L. et al	single layer	-	C, rGO and similar	-	-	-	$g \approx 2$
[S1] Seo, H.-K. et al	TEM: single to few-layer	-	C – graphene, multilayer graphene	from 0.14 MΩ·cm to 0.043 MΩ·cm	-	D ~1350 G ~1580 2D ~ 2700	-
[S2] Ruifeng Lu et al	Single layer Calculated	-	DFT calculated: 2 Li atoms per ring of C atoms	-	~6.4 wt% at 100bar 298K	-	-
[S3] A. Calka et al	HRTEM: < 20 nm thickness	-	XRD: Graphite	-	0.61wt% - 2.72 wt%, ball milled	-	-
Supl 4	HRTEM ~5nm	-	Thermally expanded GO	-	0.01 wt% 4MPa, 298K – 1.7 wt% 5.5 MPa 77K	-	-

Supplementary References

[S1] Seo, H.-K. et al. Value-added Synthesis of Graphene: Recycling Industrial Carbon Waste into Electrodes for High-Performance Electronic Devices. Sci. Rep. 5, 16710;
DOI: 10.1038/srep16710 (**2015**).
URL: http://www.nature.com/articles/srep16710

[S2] Ruifeng Lu, Dewei Rao, Zelin Lu, Jinchao Qian, Feng Li, Haiping Wu, Yaqi Wang, Chuanyun Xiao, Kaiming Deng, Erjun Kan, and Weiqiao *J. Phys. Chem. C*, **2012**, *116* (40), pp 21291–21296
DOI: 10.1021/jp308195m
URL: http://pubs.acs.org/doi/abs/10.1021/jp308195m

[S3] A. Calka , D. Wexler and T.Fenwick, Appl. Crystallogr. XX pp 219-224
DOI: 10.4028/www.scientific.net/SSP.130.219
URL: http://citeseerx.ist.psu.edu/viewdoc/download?doi=10.1.1.428.7568&rep=rep1&type=pdf

[S4] Qingrong Zhenga, Xuewen Jib, Shuai Gaoa, Xiaohua Wang Int. J. Hydrogen Energy Volume 38, Issue 25, 21 August **2013**, Pages 10896–10902,
DOI: 10.1016/j.ijhydene.2013.01.098

URL: http://www.sciencedirect.com/science/article/pii/S0360319913002073?np=y